Since January 2020 Elsevier has created a COVID-19 resource centre with free information in English and Mandarin on the novel coronavirus COVID-19. The COVID-19 resource centre is hosted on Elsevier Connect, the company's public news and information website.

Journal of Saudi Chemical Society (2022) **26**, 101531

King Saud University

Journal of Saudi Chemical Society

www.ksu.edu.sa
www.sciencedirect.com

ORIGINAL ARTICLE

Surface-Enhanced Raman Spectroscopy (SERS) for characterization SARS-CoV-2

Javier Christian Ramirez-Perez [a,*], **Daniele Durigo** [b]

[a] *Institute of Physics, São Paulo University, Rua do Matão 1371, São Paulo, 05508-090, Brazil*
[b] *Institute of Biomedical Sciences, São Paulo University, São Paulo, Brazil*

Received 15 February 2022; revised 23 July 2022; accepted 1 August 2022
Available online 13 August 2022

KEYWORDS

SARS-CoV-2;
Virus;
Surface-enhanced Raman Spectroscopy;
SERS;
Silver nanoparticles;
Detection

Abstract We used SERS with silver nanoparticles (AgNPs) as the active substrate to develop a, simple, quick, and accurate method for the detection and characterization SARS-CoV-2 without the need for RNA isolation and purification. Inactivated SARS-CoV-2 was used. The SERS signals were more than 10^5 times enhanced than the normal Raman (NR) spectra. The SERS spectra of SARS-CoV-2 fingerprint revealed pronounced intensity signals of nucleic acids; aromatic amino acid side chains: 1007 cm^{-1} (Phe marker), 1095 cm^{-1} (CN and PO_2^- markers), 1580 cm^{-1} (Tyr, Trp markers). Vibrations of the protein main chain: 1144 cm^{-1} (CN and NH_2 markers), 1221 cm^{-1} (CN and NH markers), 1270 cm^{-1} (NH_2 marker), 1453 cm^{-1} ($CHCH_2$ marker). All of these biomolecules could be adsorbed on the AgNPs surface's dense hot patches. The intensity of the SERS band varied with the concentration of SARS-CoV-2, with a virus detection limit of less than 10^3 vp/mL and RSDs of 20 %.

1. Introduction

Coronaviruses get their name from the outer fringe, crown, or "corona" of envelope protein that they have embedded. (Graphical abstract). Members of the Coronoaviridae family are responsible for a wide range of animal and human diseases. Since 2003, coronaviruses began to attract broad interest with the zoonotic SARS-CoV. Following that, the appearance of MERS-CoV in 2012 confirmed coronaviruses as major causes of severe respiratory disease [1–3]. The severe acute syndrome coronavirus 2 (SARS-CoV-2) causes the current coronavirus infection disease-2019 (COVID-19) pneumonia, which has spread worldwide and poses a serious health hazard to humans. The corona viral genome encodes four major structural proteins, a large nucleocapsid (N) protein and three transmembrane proteins are incorporated into the viral lipid envelope: the spike (S), membrane (M) and the envelope (E), all of which are required to produce a structurally complete viral particle, individually, each protein primarily plays in the structure of the virus particle, but they are also evolved in other aspects of the replication cycle [15]. SARS-CoV-2 is transmitted through respiratory droplets [4–7] and aerosols via person-to-person contact [8,9]. The development of

* Corresponding author.
E-mail address: jperez@if.usp.br (J.C. Ramirez-Perez).

Peer review under responsibility of King Saud University. Production and hosting by Elsevier.

Production and hosting by Elsevier

https://doi.org/10.1016/j.jscs.2022.101531

improved diagnostics is the major means of preventing the spread of the SARS-CoV-2 virus in the absence of a vaccine or generally effective and relevant treatments. Alternative detection, identification, and diagnostic procedures that can work alone or in conjunction with existing methods are still a priority. Currently, the methods for SARS-CoV-2 detection include electron microscopy (EM), real-time reverse transcription quantitative polymerase chain reaction (RT-qPCR) and serological enzyme-linked immune-sorbent assay (ELISA) [7,9]. However, EM is used only with limit detection around 105 particles per millilitre [10], RT-qPCR targeted viral specific RNA fragment with specific primers for the open reading frame1ab (CDDC-ORF), nucleocapsid protein (CDDC-N), envelope protein, membrane protein, or RNA-dependent RNA polymerase (RdRp) [5–9]. For RT-qPCR, RNA extraction from swab samples is required, which necessitates time-consuming pre-treatment that can take up to 4 h, posing a hurdle to SARS-CoV-2 diagnosis [8–10]. Furthermore, ELISA is a widely utilized enzyme immunoassay for detecting a receptor utilizing antigen-specific antibodies that target immunological markers such as IgM and IgG antibodies [7,8,10]. Nonetheless, for the diagnosis of SARS-CoV-2 in human and environmental samples that lack immunological markers, this technique is still time-consuming and ineffective [9,10]. Raman spectroscopy is a vibrational spectroscopy of ability to detect chemical bonds via photon scattering, although the generated signals are extremely weak in comparison to the incident beam [10,11]. SERS is a contemporary spectroscopic technique in which the Raman signal of a Raman-active molecule's functional group is considerably amplified when the molecule is adsorbed on the surface of specially prepared coinage metals, such as Ag, Au, or Cu. [11,12]. The SERS amplification is caused by two separate phenomena: first, the traditional near-field electromagnetic effect, and second, the chemical effect [13], which allows for the detection of biomolecules' local composition at extremely low concentrations (down to a single molecule) [13,14]. Furthermore, when the energy of an electronic transition is equivalent to the excitation source, the SERS approach delivers an amplification of several orders of magnitude. Signal enhancements as high as 10^{14} times over normal Raman scattering have been reported [14]. Hence, a rapid, simple, accurate and reproducible method for characterization and detection of SARS-CoV-2 is extremely required in order prevent and to tackle the spread of this deadly disease. SARS-CoV-2 is an enveloped virus with a positive sense, single-stranded RNA genome.. A few studies have been reported in the literature. For example, Turnip Mosaic virus (TuMV) coat protein prepared using silver colloid solution, the SERS bands recorded in the region (300–1700 cm^{-1}) assigned nucleic acids and amino acids [17]. Fan et et al. have used SERS technique to identify-seven food- and waterborne viruses, including norovirus, adenovirus, parvovirus, rotavirus, coronavirus, paramyxovirus, and herpersvirus. They were able to characterizeluate typical biomolecules of cells, such as nucleic acids, proteins, and amino acids, as well as other components of viruses. Using dried samples deposited onto AuNPs with covered silicon wafers. Using PCA, they were also able to identify between viruses with and without an envelope. In addition, they were able to attain a viral detection limit 10^2 vp/mL [18]. SERS signals were acquired using a silver nanorods array functionalized with the cellular receptor angiotensin-converting enzyme 2 (ACE2), which were combined with multivariate analysis to diagnose SARS-CoV-2 in environmental specimens [7]. In this study, we presented the viability of employing SERS in combination with AgNPs substrates to detect SARS CoV-2 as a diagnostic approach that is rapid, non-invasive, and has good reproducibility and accuracy, as an alternative to existing biological tests.

2. Methods

2.1. Acquisition and processing samples

SARS-CoV-2 samples were collected from the department of Microbiology, Institute of Biomedical Sciences (IBS) at University of Sao Paulo, Brazil. Previously, NP swabs were collected in a tube containing a few millimeters of viral transport medium (VTM) from three patients with confirmed COVID-19 infection in August 2020, according to an IBC-approved methodology; all samples were SARS-COV-2 positive by RT-qPCR analysis. At the Nuclear and Energy Research Institute (IPEN), viral cells were inactivated by gamma irradiation ($5x10^6$ rad). A stock SARS-CoV-2 viral cells solution was set up at concentration of $1x10^5$ vp/mL for each sample and stored at −80 °C. A total of 12 SARS-CoV-2 samples were analysed in the SERS experiment from August to September 2020. Each SERS spectrum was averaged from 18 different spots from a single sample. Gamma radiation is an ionizing radiation that is often used to render high-risk group viruses dormant in maximum containment laboratories. It's also the best way to keep viral morphology and protein structures intact [20,21]. A minimum dose of 1 Mrad (10 kGy) was recently reported to inactivate $10^{6.5}$ $TCID_{50}$/ml (tissue culture infectious dose) with negligible influence on subsequent polymerase chain reaction (PCR) assay in SARS-CoV-2 [21], but whether this claim is accurate for SARS-CoV-2 requires more investigation. The sample SARS-CoV-2-SERS-AgNP active substrate was prepared by 0.35 μL drop of SARS-CoV-2 onto AgNPs substrate, the mixture ratio of the sample and AgNPs was 1:4, the diameter of the active substrate was approximately 2 mm. In this study we proposed an experimental procedure of SERS technique for identification, detection and diagnostic of SARS-CoV-2 (Fig. 1).

2.2. Limit of detection dilution sample preparation

The limit of detection (LOD) of SARS-CoV-2 was performed by sequentially diluted from 10^5 vp/mL SARS-CoV-2 sample concentrate viral cells particle stock solution to 10^2 vp/mL diluted in 1:10, 1:100 and 1:1000 ratios using ultrapure water (nuclease-free molecular biology grade (#20022103), Austin, TX-USA). Samples were further stored at −80 °C, before SERS analysis in order to achieve a detection sensitivity of SARS-CoV-2.

2.3. Preparation of silver nanoparticles-SERS active substrates

Silver nanoparticles (AgNPs) were synthesized by reduction of silver nitrate ($AgNO_3$) solution with sodium citrate based on the method reported by Lee and Meisel [22].

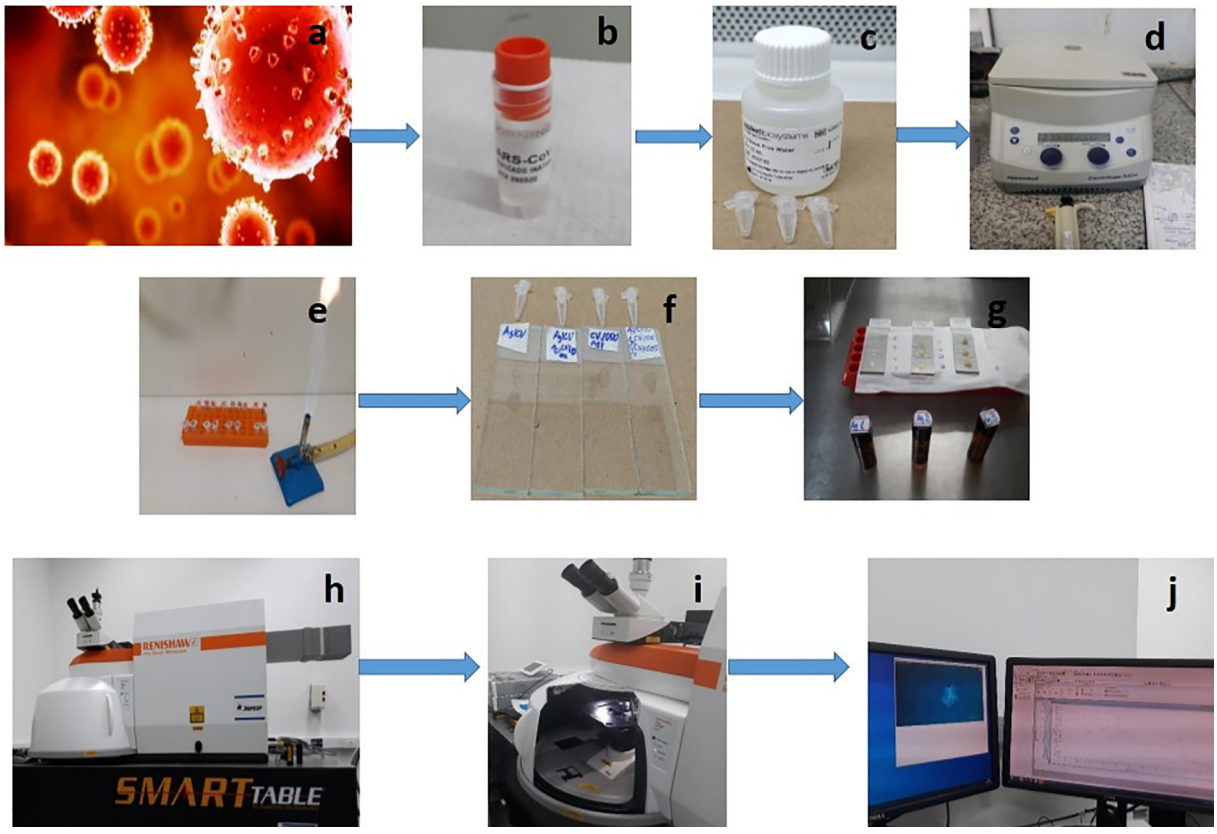

Fig. 1 The experimental set up for the SERS tests is represented schematically in this diagram: (a) SARS-CoV-2 illustration; (b) Inactivated SARS-CoV-2 sample; (c) Water, nuclease-free molecular biology grade; (d) Centrifugation of sample; (e) SARS-CoV-2 sample preparation; f) Control SARS-CoV-2 sample spiked on CaF_2 glass slide; g) SARS-CoV-2 mixed into AgNPs aggregates (SARS-CoV-2-AgNPs active substrate) cast dried thin film; (h) Renishaw Raman system equipped microscopy and 785 diode laser source; (i) Microscopy sample stage; (j) SERS spectrum of SARS-CoV-2.

Briefly, in 500 mL distilled water, 90 mg of $AgNO_3$ was dissolved. The solution was brought to a boil. The solution was then given a 10 mL aliquot of 1 percent sodium citrate and kept boiling until the volume was reduced to half of what it had been. The SAXS method is utilized to measure the average size of the nanoparticles (60 nm), and its complete structural characterization, including electron microscopy pictures, has previously been published [12,35]. In the supplementary material (Fig. 1SA, 1SB) a small aliquot of AgNPs stock solution was diluted with distilled water, and the UV–vis absorbance measurement revealed a characteristic peak of AgNPs at 390 nm. All of the samples were using the AgNPs that were synthesized.

2.4. Surface-Enhanced Raman Spectroscopy measurements spectral acquisition

SERS measurements were acquired using a Renishaw inVia Reflex Raman Microscopy System Leica DM2500 M (Renishaw PlC., New Mills, Wotton-under-Edge Gloucestershire, UK) equipped with 500 mW maximum high power, diode laser emitted a 785 nm line which was used as an excitation source. The laser light was focused on a sample mounted on a tridimensional stage with a 50x objective lens (numerical aperture (NA) = 0.75) that concentrated the laser to a spot size of roughly 2.5 μm after passing through a line filter. A 1040 × 256 pixels Peltier-cooled RenCam CCD array detector, which allowed registering the Stokes part of Raman spectra with 5–6 cm^{-1} spectral resolution and 2 cm^{-1} wavenumber accuracy, The Raman scattering signals were recorded using a 1200 line network of diffraction that was thermoelectrically cooled.. The instrument was calibrated using a silicon wafer with the band center at 520 cm^{-1}. The Raman shift range has been set from 550 to 1700 cm^{-1} (static mode) and 300 to 3500 cm^{-1} (extended mode) (SynchroScan mode), because these areas have interesting SARS-CoV-2 bands. The exposure time was 10 s, 10 accumulations, with the power of the laser set to 1 % (equal to 5mW or less), (Fig. 1).

2.5. Data processing

The OriginPro 2018.64 bit software was used to treat the NR and SERS spectra in this investigation. The AgNPs SERS active substrate was calibrated using pMBA typically standard SERS analyte, because it tends to adsorb efficiently on AgNPs surface [27]. The SERS active-substrate exhibits high sensitivity, an enhancement factor approximately 4.4 × 10^7, reproducibility (relative standard deviation, RSD = 4 %) and

stability of near 2 months of the recorded SERS spectra Fig. 3S and 4S (SM). Pre-processing of SERS spectra was done according to a procedure for spectroscopic methods to examine bilological materials that was approved [36].

Briefly, data pre-processing: A) Data pre-rubber band baseline correction substracts a rubber band, which is stretched bottom up ar each spectrum, eliminating slopes. B) De-noise the spectra depending on the SNR of the spectra, considering using Savitzky-Golay algorithm. Differentiation (Savitzki-Golay) (SG) method) has the advantage of eliminating slopes while also resolving ovelapped bands as well as smoothing, minimum noise fraction. C) Perform data normalization, this can be done using min–max normalization (e.g. normalization to the AmideI/II peak, forces all spectra to have the same a Raman intensity at the amide I/II peak. Scale the varialbles: this could be done by normalization to a 0 – 1 range.

3. Result and discussion

3.1. Features of SERS spectrum and normal Raman of SARS-CoV-2

The SERS technique was employed for the characterization and detection of SARS CoV-2. The average of 12 SERS spectra of SARS-CoV-2-AgNP substrate samples acquired during the period from 08 to 14 to 09-23-2020 are shown in Fig. 2 in perspective. The SERS spectra of SARS-CoV-2 exhibits a number of marker modes spreading well all over the region between 1000 and 1700 cm^{-1}. Except the obvious minor differences in intensities, orientations and peak sharpness in relative band width and intensity, the SERS spectra obtained over the period of testing were identical in the spectral region 500–1700 cm^{-1}.The SERS spectra have a high sensitivity, a signal amplification of up to $7.0x10^5$, and are reproducible across the period of time testing. Large enhancement factors of the electromagnetic field are only accomplished in very tiny areas of the surface of nanostructured metals, due to the increased degree of AgNP aggregation, which is critical for forming efficient "hot spots." [14,19]. Because of the high density of the hotspots, only a tiny percentage of SARS-CoV-2 biomolecules are adsorbed on junctions of two or more AgNPs resulted in a significantly increased and reproducible SERS signal [23]. SARS-CoV-2 with and without spike AgNPs was firstly tested as a proof-of-concept demonstration of the protocol developed in this study. Fig. 3Aa and 3Ba show example Norma Raman (NR) spectra tests in the spectral region of 500 to 1700 and 300–3500 cm^{-1}, respectively. The recorded NR spectra were highly reproducible, and reveal no signal besides a weak band with maximum c.a. 1400 cm^{-1} comparing to the incident beam. The Raman intensity in the NR spectra without AgNPs varies between 2 and 5×10^2. Correspondingly, the NR spectrum of clean CaF_2 glass slide used as platform to spot the SARS-CoV-2 sample (Fig. 3Ab and Fig. 3Bb) exhibits no signal, possibly as a result of the SARS-CoV-2 viral suspension sample's transparency, CaF_2 was utilized as the window material in order to eliminate multiple internal reflections. In contrast, the SERS spectra of SARSCoV-2 measurements in the spectral region between 1000 and 1700 cm^{-1} indicate pronounced band enhancement, especially the SERS signals centered around 1000 cm^{-1} (Fig. 3Ac and 3Bc), which shows highly reproducible bands with great uniformity and extraordinary sensitivity. The orientation on the surface of aggregated

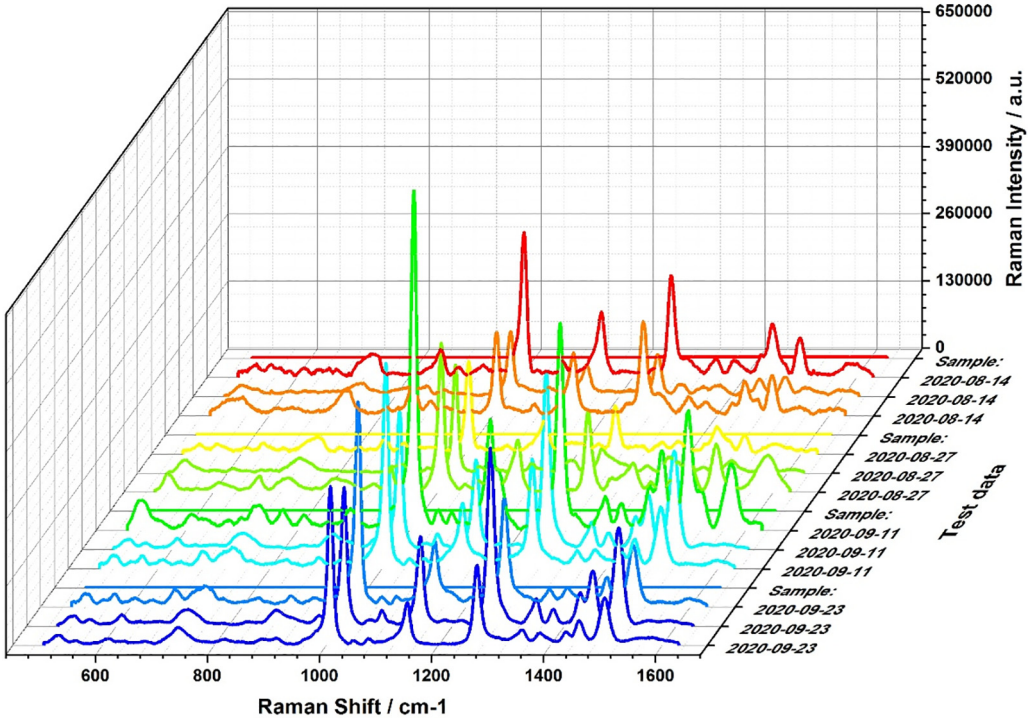

Fig. 2 The representative of three-dimensional SERS spectra during the period of August 14 to September 23, 2020, the average SERS spectra of 12 samples of SARS-CoV-2 virus cells. SERS spectra were averaged from 18 different spots on a single sample for each spectrum.

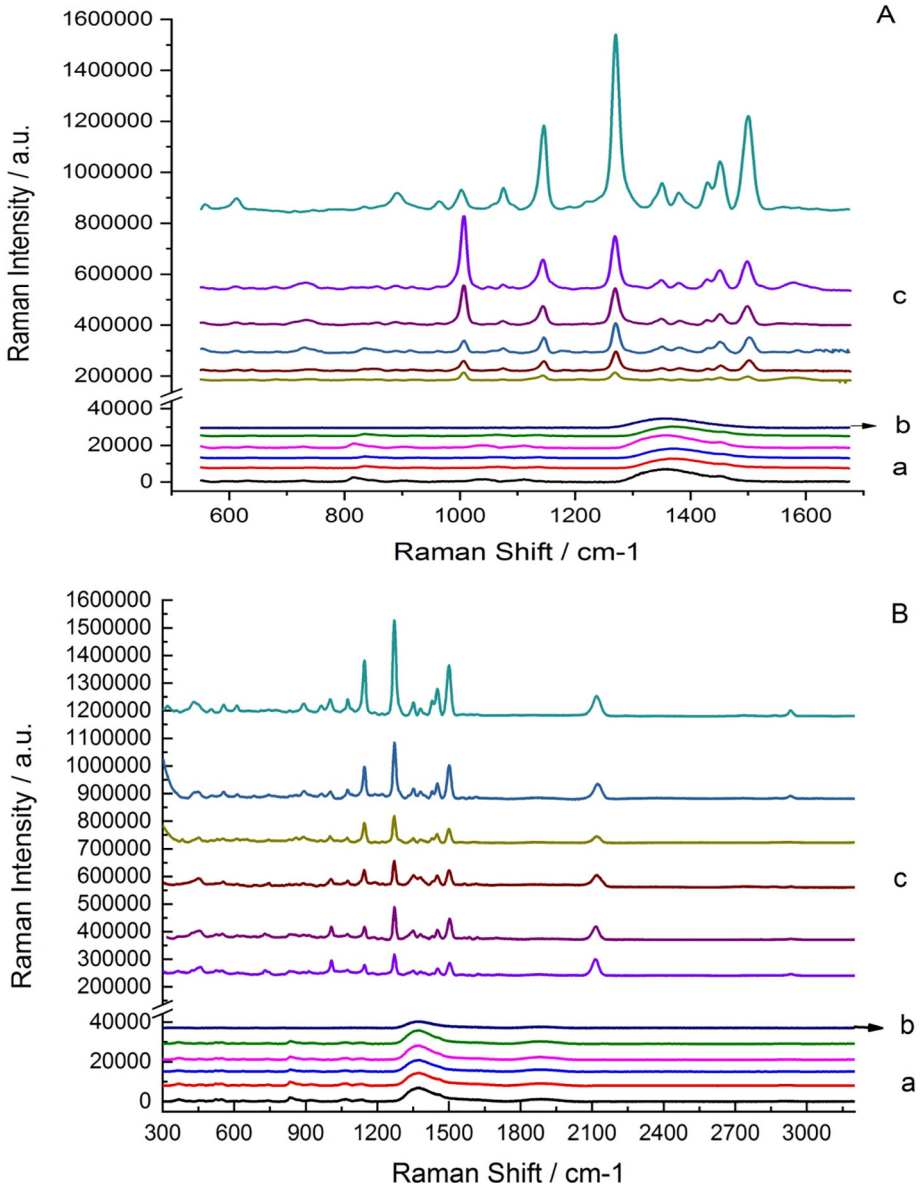

Fig. 3 The representative Raman/SERS spectra in the regions A) 500–1700 cm^{-1}; and B) 300–3500 cm^{-1} region. are compared. Aa) and Ba) NR without AgNPs; Ab) and Bb) Clean Ca_2F glass slide; Ac) and B-c) SARS-CoV-2- AgNPs-SERS substrate.

AgNPs could also explain the adsorption of several amino acids with cyclic R side chains, such as aromatic ring in phenylamine at 1007 cm^{-1}. As can be shown, our SERS-active substrate achieves a substrate with a very high enhancement magnitude, ranging from 0.2 to 1.6 × 10^6 (Raman Intensity). However, some bands in the SERS spectra of SARSCoV-2 show fluctuation in relative band shapes and intensities in other spectral regions between 400 and 1000 cm^{-1} and 1500 to 3500 cm^{-1}, respectively. This is attributable to the fact that the SARS-CoV-2 biomolecules' adsorption behavior on AgNPs aggregates. The enhancement of the electromagnetic field in the slits between AgNPs aggregates has been reported to be much higher [16,19,23]. Thus, before SERS measurements AgNPs are usually aggregated/agglomerated to generate such slits. Low-intensity shape bands were found, as well as a lack of high signal-to-noise ratios, implying the presence of several overlapping peaks. This could be because SARS-CoV-2 includes numerous biomolecules that all co-adsorb on the surface of AgNPs, causing peak broadening. Furthermore, the orientation of the adsorbate on the hot spots generated between the intraparticle gaps of AgNPs is likely modulated by the relative low intensity of the molecular components. In section 3.4, the SERS spectra, band intensities, and marker modes recorded in the 500–1700 and 300–3500 cm^{-1} regions, respectively, are examined in better detail.

3.2. SERS reproducibility of SARS-CoV-2

A total of 9 SARS-CoV-2 SERS spectra were acquired from 3 random places on the same active substrate for varied concentrations to demonstrate the reproducibility of SARS-CoV-2 SERS spectra. The experiment was conducted by dilutions of inactivated SARS-CoV-2 (stock solution) from 10^5 vp/mL to

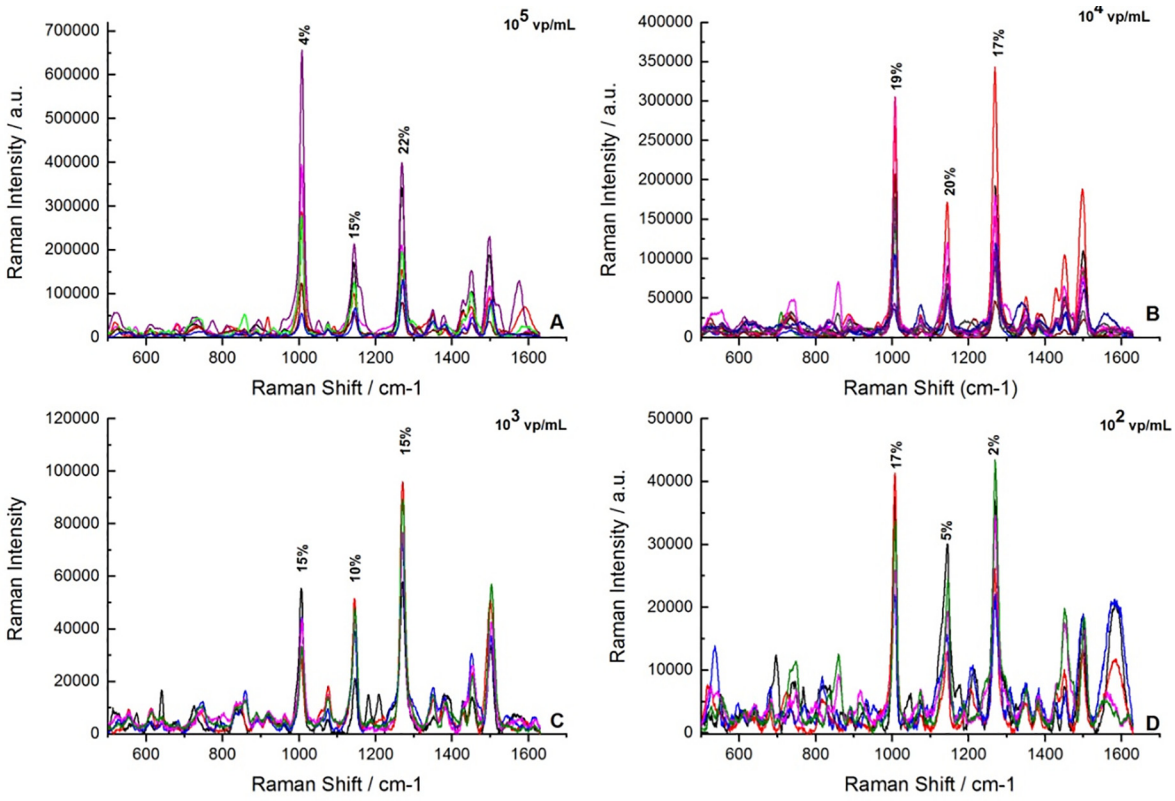

Fig. 4 The SERS spectra of SARS-CoV-2 with various concentrations and Av.STD (%) of selected bands at: 1007, 1144 and 1270 cm^{-1}: A) 10^5 vp/mL B) 10^4 vp/mL; C) 10^3 vp/mL; D) 10^2 vp/mL.

10^4, 10^3 and 10^2 (vp/mL) using ultrapure water, which served reference (Fig. 4A-D). Except for small intensity fluctuations in some bands, the SERS spectra varied with SARS-CoV-2 concentration, and the majority of the bands showed highly enhanced and reproducible SERS signals, implying the efficacy of AgNPs aggregate substrates. The excellent reproducibility could be ascribed to the virus cells'high density distribution, which indicates that most of the macromolecules of SARS-CoV-2 come into direct contact with the AgNPs' hot spots, which possible benefit to obtain a uniform SERS signal. We observed significant SERS signal enhancement with the concentration of SARS-CoV-2. For instance, high signal enhancement *ca.* 6.5×10^5 times over NR scattering is achieved for 10^5 vp/mL of SARS-CoV-2 (Fig. 4A). In the SERS spectra, we identified the most significant bands as well as their reproducibilities reported as relative standard deviations (RSDs) at: 1007 cm^{-1} (4 %); 1144 cm^{-1} (15 %); and 1270 cm^{-1} (22 %). The signal enhancement declined to *ca.* 3.5 x10^5, 1×10^5 and 4.3 x10^4 for SARS-CoV-2 concentrations of 10^4, 10^3 and 10^2 vp/mL, respectively, for each intensity, including RSDs at: 1007 cm^{-1}, 1144 cm^{-1}, and 1270 cm^{-1} detected for each intensity 1007 cm^{-1}, 1144 cm^{-1}, and 1270 cm^{-1} (Fig. 4-B-D).

For SERS quantitative research, less than 20 % variance in SERS intensity between different locations of the active substrate is acceptable [25], in agreement with our findings. In addition, the SERS spectra for 10^5 vp/mL SARS-CoV-2 concentration were recorded by mapping a small area (20 μm × 20 μm) on the slide in the range of 500 to 1700 cm^{-1} (Supporting material Fig. 4S). The high reproducibility in this investigation can be ascribed to a homogeneous mixing of SARS-CoV-2 viral suspension and AgNPs of the same size (60 nm) and shape (spherical).

3.3. Limit of detection (LOD) of SARS-CoV-2 based on SERS method

The LOD was explored by comparing SERS signal enhancement with SARS-CoV-2 concentration; for instance, for 10^5 vp/mL high signal enhancement of *ca.* 6.5×10^5 times over NR scattering was achieved (Fig. 5A). The signal enhancement declined to *ca.* 3.5×10^5, 1×10^5 and 4.3×10^4 7 for SARS-CoV-2 concentrations of 10^4, 10^3 and 10^2 vp/mL, respectively (Fig. 5B). The LOD was defined in the literature as the concentration of SARS-CoV-2 for which the strongest signal of SERS enhancement was equal to 3 times the background SERS signal intensity, with the background SERS signal intensity referring to the SERS signal from a sample with virus cells concentration of 0 [26]. In order to determine the LOD, the SERS intensities of three peaks at 1007, 1144, and 1270 cm^{-1} were notably strong and the intensity of the peaks increased when the viral cell concentration of SARS-CoV-2 increased. The peak at 1007 cm^{-1}, on the other hand, was one of the strongest for SARS-CoV-2, and its intensity increased as the concentration of SARS-CoV-2 increased. As a result, the peak at 1007 cm^{-1} was chosen as a hint vibration to estimate SARS-CoV-2 concentration and to evaluate the LOD for SARS-CoV-2 samples. The peak intensity at 1007 cm^{-1} (I_{1007}) was plotted as a function SARS-CoV-2 con-

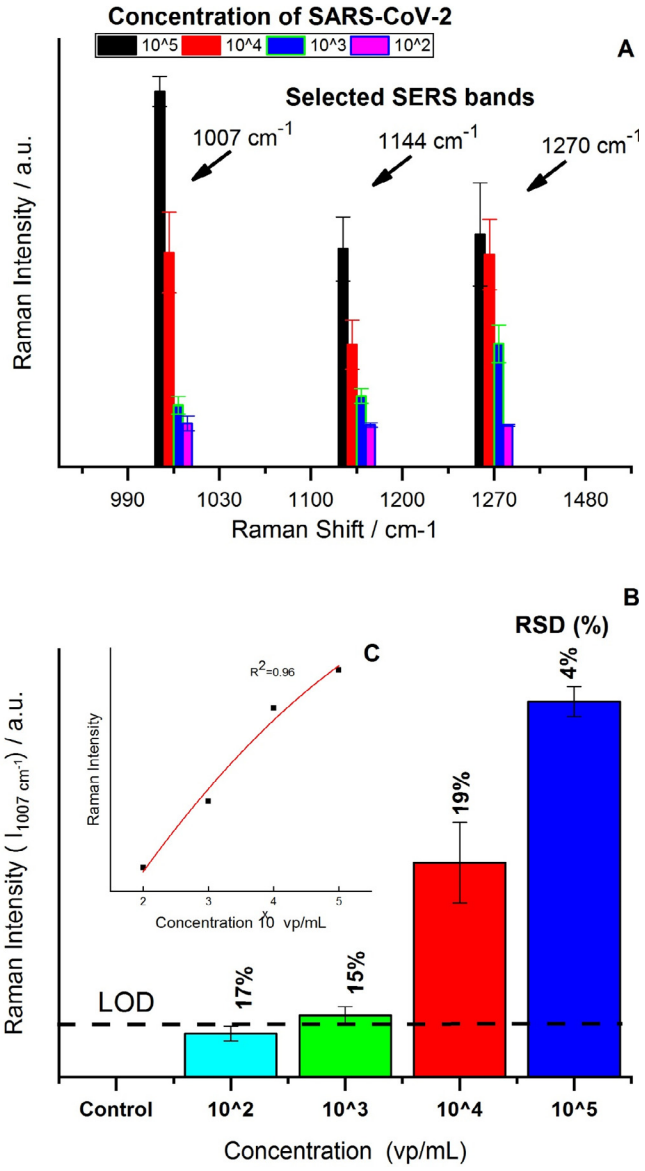

Fig. 5 A) SERS band intensities at 1007, 1144, and 1270 cm^{-1} as a function of SARS-CoV-2 concentration: 10^5, 10^4, 10^3 and 10^2 vp/mL. B) For LOD determination, the relative standard deviation (RSD %) for the selected band at 1007 cm-1 as a function of SARS-CoV-2 concentration. C) The inset shows the correlation of Raman intensity with concentration at 1007 cm^{-1}.

centration (Fig. 5C). The lowest concentration of SARS-CoV-2 found by this approach was lower than10^3 vp/mL, based on the average and 3 times of the SERS signal marked as control. The peak intensity (I_{1007}) against the concentration of SARS-CoV-2 (vp/mL) with an R^2 value of 0.96 confirming that the lowest concentration of SARS-CoV-2 detected with this assay may be around 10^3 vp/mL.

3.4. SERS characterization of SARS-CoV-2

The current investigation, which took place from August to October 2020. The SERS technique was used to explore using AgNPs, SARS-CoV-2 characterisation and detection of key

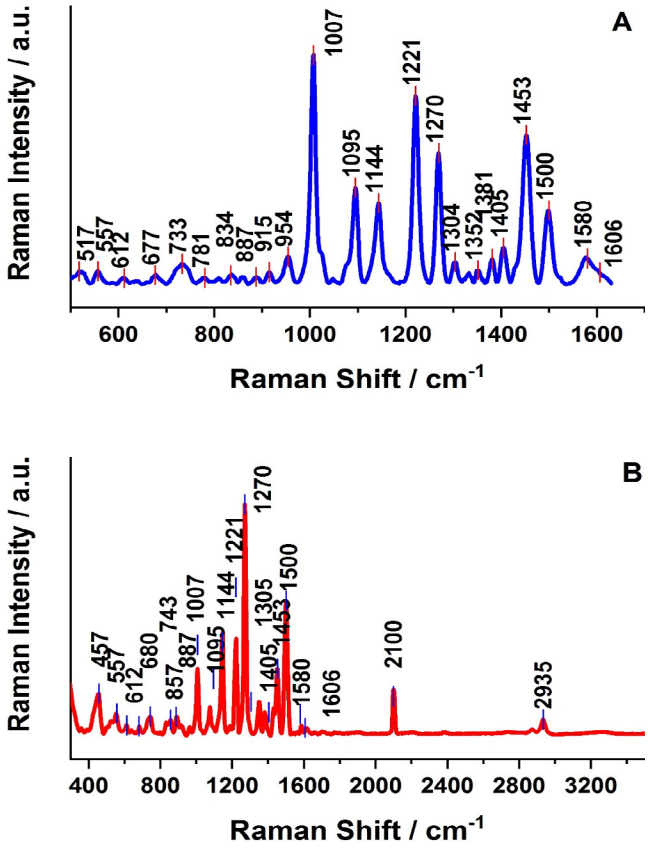

Fig. 6 The average SERS spectra of SARS-CoV-2 using AgNPs deposited onto CaF_2 glass slide platform cast dried thin film. Each SERS spectrum was obtained by averaging 18 measurements recorded at random location across the sample. The experimental conditions were: 1 % (500 mW), 785 nm excitation, 10 s exposure time. All SERS spectra were base line corrected and normalized and shifted vertically for improved visualization in the spectral range A) 500–1700 cm^{-1}; and B) 300–3500 cm^{-1}.

biomolecules such as structural proteins derived from SARS-CoV-2 composition. The average typical SERS spectra of SARS-CoV-2 mixed with aggregated AgNPs are shown in the region between 500 and 1700 cm^{-1} (Fig. 6A) and 300 and 3500 cm^{-1} (Fig. 6B), respectively. Table 1 shows the complete list of peaks wavenumber for SARS-CoV-2 as well as suitable tentative biomolecules assignments. The primary vibrational sharp and intense signals are visible in the SERS spectrum of SARS-CoV-2 at 1007, 1221, 1453 and 1270 cm^{-1}; in the mid intense at 1095, 1144, 1580 cm^{-1}; broad low intense at 1500 and 733 cm^{-1}; low intense at 1405, 954, 1381, 1304 cm^{-1}; and very low intense signals in the region between 500 and 887 cm^{-1}. The pronounced intense band centred at 1007 cm^{-1}, which is assigned to Phe marker, and the C—C skeletal stretching vibration of the phenylalanine ring combined with C—H in plane. Other vibrational modes of Phe located at 1001 cm^{-1} attributed to the symmetric ring breathing mode; 1018 and 1022 cm^{-1} assigned to the in-plane C—H bending, at 1032 cm^{-1} attributed to in-phase motion υ(C—C) and δ(C—C—H) [12]. The next intense band at 1221 cm^{-1} is ascribed to PO_2^-, NH_2 markers of amide III, which result from the coupling of υ (C—N) and δ(N—H),

Table 1 Tentative SERS bands assignments of SARS-CoV-2 main Raman shift vibrational modes.

Range (cm^{-1})		Tentative Assignments[†]
500–1700	300–3500	
=	457	r (COO–)[‡]; Phe, Tyr
517	=	υ(S—S) disulfide (amino acid cysteine) [‡]
557	557	C—C twist mode of Phe (proteins)
612	612	C—C twist mode of Phe; δ(COO–)
677	680	Tyr
733	743	A,U, T, C, ring breathing modes in the DNA/RNA
781	=	υ(O—P—O) RNA
834	857	υ_s(O—P—O) str, T
887	887	DNA/RNA, phosphodiester, deoxyribose
915	=	υ(C-COO-)
954	=	υ(C—O) and C—N of proteins
1007	1007	δ(C—C) aromatic ring in Phe
1095	1095	υ(C—N), υ(PO_2^-) nucleic acid,
1144	1144	C—N streching in proteins, t(NH_2)
1221	1221	Amide III, υ as (PO_2^-), δ(NH_2)
1270	1270	Amide III, δ(NH_2)
1304	1305	Amide I, C—H def
1352	1352	A,G C—H def υ_s(COO^-)
1381	1381	ρ(C—H)
1405	1405	CH_2 sciss, G,A
1453	1453	δ($CHCH_2$), proteins and lipids
1500	1500	δ(C═C) in benzenoid ring, amide II
1580	1580	A,G (DNA/RNA), C═C bending mode of Phe υ_s(COO^-), Tyr, Trp
1606	1606	Phe ring bond vibration, in-phase motion of υ($C_δ$-$C_ε$)
=	2100	υ(C≡C), υ(C≡N), peptides residues
=	2935	υ(C—H), υ(C-H_3) membrane of lipids

[†] All the assignments are from references [18,27,28,29,30,31].
[‡] υ, stretching; δ, bending; ρ, rocking; τ, torsion; wagg, wagging; twist, twisting; sciss, scissoring; def, deformation; as, asymmetric; s, symmetric; C, cytosine; T, thymine; Aadenine; G, guanine; U, uracil; Phe, phenylalanine; Tyr, tyrosine, Trp, tryptophan.

although it has a week band in the region 300–3500 cm^{-1}, it is discernible (Fig. 6B) and has a low signal-to-noise ratio suggesting the presence of overlapping peaks. This is because SARS-CoV-2 cells contain numerous macromolecules that likely co-adsorb on AgNPs surfaces, resulting in peak reduction and distortion. Strong bands at 1070 cm^{-1} attributed to (γ—C—N) also indentified in the SERS spectra of other viruses [17,18]. Vibrational modes exist in the amide I, II and III, which are conformational sensitive. Primary C═O stretching, in-plane modes of N—H bending, and υ(C—C) vibrational modes are included in the amide groups. At 1270 cm^{-1} ascribed to NH2 marker, whis is very strong amide III mode for α-sheet disorder conformation. Band at 1268, 1286, and 1296 cm^{-1} (amide III vibration of protein α-helix structure) were identified in the SERS spectra of other viruses [17,18]. CH(CH_2) bending modes markers in proteins and nucleic acids are responsible for the next strong peak at 1453 cm^{-1}. Amino acids and purines molecules are probably to promote adsorption on hot spot located on AgNPs' surface, allowing for an enhancement in the vibration of these molecules at 1095 cm^{-1}, a medium-intense band can be assignable to the complex symmetrical mode of PO_2^- marker, which is composed of nucleic acids (Fig. 6A). However, in the SERS spectrum of Fig. 6B, this band appears to have shifted slightly to 1075 cm^{-1}, a strong band at 1070 cm^{-1} attributed to (γ—C—N) also indentified in the SERS spectra of other viruses [17,18]. This spectral shift can be attributed to the molecular layers coating the AgNPs, and the relative intensity of the molecular components is modulated by the orientation of the adsorbate onto the AgNPs surfaces. The next medium-intense bands appear at 1144 cm^{-1} which correspond to C—N stretching proteins marker, and at 1500 cm^{-1}, which is due to the presence of amide II υ(C═C) in benzenoid ring, indicating that SARS-CoV-2 molecules are adsorbed to AgNPs carboxyl groups and other molecules related to amino groups. The ring breathing modes in purine DNA/RNA are assigned to the low-broad intense at 733 (Fig. 6A) and 743 (Fig. 6B), probably from building blocks created during amino acid catabolism. A virion (also called a virus, or particle) is made up of DNA or RNA molecules surrounded by a protective coat of proteins [32]. Tyr, Trp, Adenine, Guanine (DNA/RNA); C═C bending mode of Phenylalanine markers, can also be ascribed to the next low-broad intensity at 1580 cm^{-1} [33,34]. Low intensity band at 1405 cm^{-1} in the 1300–1650 cm^{-1} region attributable to CH_2 scissoring, shifted to 1430 cm^{-1}, attributed to adenine or guanine, the band at 1606 cm^{-1} from the phenyl ring bond-stretching vibrations, assigned to in-phase motion of υ($C_δ$-$C_ε$). Low-intensity bands at 1304, 1352, and 1381 cm^{-1} (Fig. 6A) were ascribed to Amide III (protein) cytosine, purines (T,A,G), and tryptophan.. The next low intensity bands are seen at 954 and 915 cm^{-1} which correspond to the proteins υ(C—O) and C—N and υ (C-

COO^-). Interestingly, too weak bands (low intensities) at 887, 834, 857, and 781 cm^{-1} are due to phosphodiester, (O—P—O) stretching of thymine and RNA moieties in the deoxyribose molecule. Other low weak intensity bands at 577, 612, 677 and 680 cm^{-1} were attributed C—C twisting mode of phenylalanine and adenine, purines. Furthermore, we discovered a peak at 517 cm^{-1}, which is assigned to the protein's S—S stretching modes of cysteine residues in proteins, the band at 612 cm^{-1} appears in the Raman spectra of proteins as Phe ring breathing vibration corresponding to a homothetic motion of the ring breathing atoms C—C twist. Finally, the remaining two bands the first at 457 cm^{-1} assigned to amino acids with a cyclic R side, such as Phe or Trp, suggesting that the carboxyl groups-r(COO^-) are chemically adsorbed to AgNPs [19,17]. The appearance of the band at 2100 cm^{-1} in our samples is most likely due to dehydration of the peptide bond, which results in results in υ(C≡C) or υ(C≡N) due to degradation (peptide and protein residues) caused by laser power. The last band at 2935 cm^{-1} can be assigned to asymmetric and symmetric CH_3 stretching vibrations of the methyl end groups of membrane lipids as well as the methyl side groups in cellular proteins. These molecules are most likely derived from E and S SARS-CoV-2 proteins associated with glycoproteins, which includes a bilayer lipid envelope outside the protein coat. (Fig. 6B, and Table 1). Using highly SERS active aggregated AgNPs substrate to identify SARS-CoV-samples, adsorption of biomolecules including proteins, peptides of SARS-CoV-2 onto the surface of AgNPs depends on the chemical origin of the biomolecules and SERS enhanced mechanism, which entails changes in frequency and intensity that are primarily related to the distance between AgNPs colloids and groups of SARS-CoV-2 biomolecules.

4. Conclusion

A novel, simple, quick, and accurate technology for acquiring strong, sharp, and reproducible SERS signal intensities was developed. When compared to normal Raman spectra, the SERS approach resulted in an intensity enhancement of over 10^5 fold. The SERS spectra obtained using the experimental protocol developed exhibited significant consistency, sensitivity and selectivity. We also studied the spectral reproducibility and virus detection limit of SARS-CoV-2 virus SERS spectra at different concentrations 10^2 and 10^5 vp/mL, and the LOD achieved lower than 10^3 vp/mL. RSDs of less than 20 %. The major vibrational sharp and intense signal in the SERS spectrum of SARS-CoV-2 was found at 1007, 1221, 1270, and 1453 cm^{-1} in the 500–1700 cm^{-1} range, and 457 and 2395 cm^{-1} in the 300–3500 cm^{-1} region. Furthermore, these bands were ascribed to typical biomolecules found in the major structural proteins of SARS-CoV-2. The most prominent bands from nucleic acids were identified by the SERS spectra of the SARS-CoV-2 fingerprint: aromatic amino acid side chains: 1007 cm^{-1} (Phe marker), 1095 cm^{-1} (C—N and PO_2^- markers), 1580 cm^{-1} (A, G, Tyr, Trp markers). Vibrations of the protein main chain: 1144 cm^{-1} (C—N and NH_2 markers), 1221 cm^{-1} (CN and NH markers), 1270 cm^{-1} (NH_2 marker), 1453 cm^{-1} ($CHCH_2$ marker). Development of improved detection and characterization is primarily means of controlling SARS-CoV-2 virus infection spread everywhere, in order to battle COVID-19 infectious disease. Finally, the SERS technique we proposed for detecting, characterizing and monitoring of SARS-CoV-2 variants is quick, precise, and cost-effective with high sensitivity.

Declaration of Competing Interest

The authors declare that they have no known competing financial interests or personal relationships that could have appeared to influence the work reported in this paper.

Acknowledgements

The authors gratefully acknowledge the support of the Research Unity in Astrobiology NAP-Astrobio/IAG-University of Sao Paulo-Brazil for allowing us to use the Rainshaw Raman Equipment for this research.

Funding

N/A.

References

[1] N. Ramadan, H. Shaib, Middle east respiratory syndrome coronavirus (MERS-COV): A review 2019. In GERMS, https://doi.org/10.18683/germs.2019.1155, Accessed on 4 Dicember 2021.
[2] D. Sohrabi, Z. Alsafi, N. O'Neill, M. Khan, A. Kerwan, A. Al-Jabir, C. Losifidis, R. Agha, WHO declares global emergency: A review of the 2019 novel coronavirus (COVID-19), Int. J. Surgery (2020), https://doi.org/10.1016/j.ijsu.2020.02.034.
[3] Y. Wang, Y. Wang, Y. Chen, Q. Qin, Unique epidemiological and clinical features of the emerging 2019 novel coronavirus pneumonia (COVID-19) implicate special control measures, J. Med. Virol. 92 (6) (2020) 568–576.
[4] World Health Organization [Online]. Available at: https://www.who.int/docs/default-source/coronaviruse/situation-reports/20201020-weekly-epi-update-10.pdf.
[5] C-C. Lai, T-P. Shih, W-C. Ko, H-J.Tang, P-R Hsueh, Severe acute respiratory syndrome coronavirus 2 (SARS-CoV-2) and coronavirus disease 2019 (COVID-19): The epidemic and the challengues. Int. J. Antimicrob. Agents. 55 (2020) 105924.
[6] F. Xiao, M. Tang, X. Zheng, Y. Liu, H. Shan, Evidence for gastrointenstinal infection of SARS-CoV-2, Gastroenterology 158 (2020) 1831–1833.
[7] D. Zhang, X. Zhang, R. Ma, S. Deng, X. Wang, X. Zhang, X. Huang, Y. Liu, G. Li, J. Qu , Y. Zhu, J. Li, Ultra-fast and onsite interrogation of Severe Acute Respiratory Syndrome Coronavirus 2 (SARS-CoV-2) in environmental specimens via surface enhanced Raman scattering (SERS). medRxiv (2020), hppts://doi.org/10.110/2020.05.0220086876.
[8] M.L. Holshue, Novel coronavirus in the United States, N. Engl. J. Med. 382 (2020) 929–936, https://doi.org/10.1056/NEJMoa2001191.
[9] D. Wang, B. Hu, C.Hu. Z.Fangfang, X.Liu, J. Zhang, Z.Peng, Clinical Characteristics of 138 Hospitalized patients with 2019 novel coronavirus-infected Pneumonia in Wuhan China. JAMA 33 (2019) 1061–1069.
[10] S. Stöckel, J. Kirchhoff, U. Neugebauer, P. Rosch, J. Popp, The Application of Raman spectroscopy for the detection and identification of microorganisms. Review, J. Raman Spectroscopy 47 (2016) 89–109.

[11] S. Bahavya, R.F. Renee, H. Anne-Isabelle, R. Emile, PVD., Richard, SERS: material, applications, and the future, Materials 15 (2012) 16–115.
[12] J.C. Ramirez-Perez, T. Alves dos Reis, M. Rizzutto,Identifying and detecting Entomopathogenic fungi using SERS BAJER, 4 (4) (2021) 4832-4350, https://doi.org/10.34188/bjaerv4n4-002.
[13] T. Zhong-Q, Y. Zhi-Lin, R. Bin, W. De-Yin, SERS from transition metals and exited by ultraviolet light, in: K. Katrin, K. Herald, M. Martin (Eds.), Surface-enhanced Raman Scattering Physics and Applications, first ed., Springer-Verlat Berlin Heidelberg, Germany, 2006.
[14] M. Moscovits, Surface-enhanced spectroscopy, Rev.Mod. Phys. 57 (1985) 783–826.
[15] D. Shoeman, C.F. Burtram, Coronavirus envelope protein; current knowledge, Virol. J. 16 (69) (2019) 1–22.
[16] Z. Ke, J. Oton, Qu K., M. Cortese, V. Zila, L McKeane, T. Nkane, J. Zlvanov, C. Neufeldt, B. Cerlkan, R. Bartenschlager, J.A. Briggs, Structures and distribution of SARS-CoV-2 spike proteins o intact virions. Nature, article, 1 (2020) 1-25. https://doi.org/10.1038/s41586-020-2665-2.
[17] X.Y. Zhang, M.A. Young, O. Lyandres, R.P. Van Duyne, Rapid detection of an anthrax biomarker by surface-enhanced Raman spectroscopy, J. Am. Chem. Soc. 127 (12) (2005) 4484–4489.
[18] C. Fan, Z. Hu, L.K. Riley, G.A. Purdy, A. Mustapha, M. Lin, Detecting food-and waterborne viruses by surface-enhanced Raman spectroscopy, J. Food Sci. 75 (5) (2010) 302–307.
[19] P.D. Bao, T.-Q. Huang, X.-M. Liu, T.-Q. Wu, Surface-enhanced Raman spectroscopy of insect nuclear polyhedrosis virus, J. Raman Spectrosc. 32 (2001) 227–230.
[20] F. Feldman, W.L. Shupert, E. Haddock, B. Twardoski, H. Feldmann, Gamma irradiatin as an effective method for inactivation on emerging viral pathogens, Am. J. Trop. Med. Hyg. 100 (5) (2019) 1275–1277.
[21] A. Leung, K. Tran, J. Audet, S. Lavineway, N. Bastien, J. Krishman, In vitro inactivation of SARS-CoV-2 using gamma radiation, Appl. Biosafety: J. ABSA Int. (2020) 1–4, https://doi.org/10.1177/1535676020934242.
[22] P.C. Lee, D. Meisel, Adsorption and surface-enhancement Raman of dyes on silver and gold sols, J. Phys. Chem. 86 (1982) 3391–3395.
[23] K. Kneipp, Y. Wang, H. Kneipp, L.T. Perlman, I. Itzan, R.R. Dasari, M.S. Feld, Approach to single-molecule detection using surface-enchanced resonance Raman-scattering (SERRS)-a study using Rhodamine 6G on colloidal silver, Appl. Spectrosc. 49 (1997) 780–784.
[25] Wang, H-H., Liu, CC., Wu, SB., Liu NW., Peng, CY, Highly Raman enhancing substrates based on silver nanoparticle arrays with tunable sub-10 nm gaps Adv. Mater. 18 (4) (2006)491–495.
[26] A. Rygula, K. Majznere, K.M. Marzec, A. Kaczor, M. Pilarczyk, M. Baranska, Raman spectroscopy of proteins: a Review, J. Raman Spectrosc. 44 (2013) 1061–1076.
[27] H. Wei, A. McCarty, J. Song, W. Zhou, P.J., Vikesland, Quantitative SERS by hot spot normalization – surface enhanced Rayleight band intensity as an alternative evaluation parameter for SERS substrate performance, Faraday Dicuss, 205 (2017) 491-504, https//doi.org/ 10.103/9/c7d00125h.
[28] H. Deng, Q. He, The study of Turnip Mosaic virus coat protein by surface enhanced Raman spectroscopy, Spectrochim. Acta 49 (12) (1993) 1709–1714.
[29] S.A. Eichorst, F. Strasser, T. Woyke, A. Shcintlmeister, M. Wagner, D. Woebken D, Advancement in the application of NanoSIMS and Raman microspectroscopy to investigate the activity of microbial cells in soils, FEMS Microbiol. Ecol., 91 (10) (2015)1-14. Fiv106.doi: 10.1093/femsec/fiv106.
[30] J.S. Ellis, M.C. Zambom, Molecular diagnosis of influenza, Rev. Med. Virol. 12 (2002) 375–389.
[31] D. Newman, FT-Infrared and FT-Raman Spectrosocpy in biochemical research, Appl. Spectrosc. 36 (2) (2001) 239–298.
[32] P. Hermann, A. Hermelink, V. Lausch, G. Holland, L. Möller, N. Bannert, D. Naumann, Evaluation of tip-enhanced Raman spectroscopy for characterizing different virus strains, Analyst 136 (2011) 1148–1152.
[33] P. Hermann, H. Fabian, D. Naumann, A. Hermelink, Comparative study of far-field and near-field Raman spectra from silicon-based samples and biological nanostructures, J. Phys. Chem. C. 115 (2011) 24512–24520.
[34] T. Lemma, J. Wang, K. Arstila, V.P. Hytonen, J.-J. Toppari, Identifying yeasts using surface enhanced Raman spectroscopy, Spectrochim. Acta Part A Mol. Biomol. Spectrosc. 218 (2019) 299–307.
[35] P. R.A.F., Garcirasmik, K. Pappert, W. Wlysses, L. Otubo, M. Epple, C.L.P., Olivera, An in situ SAXS investigation of the formation of silver nanoparticles and bimetallic silver-gold nanoparticles in controlled wet-chemical reduction synthesis, Nanoscale Adv., 2 (1)(2020):225–238, 10.1039/c9na00569b.
[36] M.J., Baker, J. Trevisan, P. Bassan, R. Bhargava, HJ Butler, K. M., Dorling, F.L. Martin, Using Fourier transform IR spectroscopy to analyze biological materials Nat. Protocols 9 8 10.1038/nprot.2014.110. 2014, pp. 1771–1778.

Further reading

[24] E.C. Le Ru, E. Blackie, M. Meyer, Etchegoin PG, Surface enhanced Raman scattering enhancement factors: A comprehensive study, J. Phys. Chem 111 (2007) 13794–13803.